JOURNAL OF APPLIED ELECTROCHEMISTRY **28** (1998) 907–913

Model of nickel electrodeposition from acidic medium

F. LANTELME, A. SEGHIOUER

Laboratoire d'Electrochimie, Case 51, Université Pierre et Marie Curie, 4 place Jussieu, 75252 Paris Cedex 05, France*

A. DERJA

Laboratoire d'Electrochimie, Faculté des Sciences, Université Cadi Ayyad, B.P.S 15, Marrakesh, Morocco

Received 9 June 1997; revised 17 November 1997

A step-wise computer model is presented for simultaneous deposition of nickel and nickel hydroxide in aqueous solutions. In acidic solutions (pH $\simeq$ 1), the potentiostatic current-time transient response on glassy carbon or titanium was analysed with respect to nucleation and radial growth mechanism. pH changes influence the current-time response greatly. A marked maximum in the current transient appears for slightly acidic solutions (pH $\geq$ 4.5) and a consecutive decrease in the deposition current density at long times is obtained. This behaviour is attributed to early precipitation of nickel hydroxide due to a local pH increase at the cathode surface.

Keywords: *nickel electrodeposition*, *electrocrystallization*, *modelling*, *nucleation*, *chronoamperometry*

List of symbols

$\mathscr{A}_{free}$	fractional area not covered by nickel and hydroxide
$\mathscr{A}_{Ni}$	actual fractional area covered by nickel in the presence of hydroxide
A_{OH}	fractional area covered by hydroxide without coalescence
$\mathscr{A}_{OH}$	actual fractional area covered by hydroxide
A_t	fractional area covered by nickel nuclei without coalescence at time t
$\mathscr{A}_t$	actual fractional area covered by nickel nuclei at time t
E	electrode potential (V)
E^*	equilibrium potential (V)
E°	standard potential (V)
F	Faraday constant
j_{H_2}	current density for hydrogen evolution ($A\,cm^{-2}$)
j_{Ni}	current density for the nickel deposition ($A\,cm^{-2}$)
j_t	total current density at time t ($A\,cm^{-2}$)
k	nucleation rate constant for nickel (s^{-1})
k_{OH}	nucleation rate constant for hydroxide (s^{-1})
K	preexponential factor for nickel nucleation ($s^{-1}\,V^{-2}$)
K_{OH}	nucleation factor for hydroxide ($s^{-1}\,dm^3\,mol^{-1}$)
N_t	number of nucleation sites per unit area at time t (cm^{-2})
N^0	number of nucleation sites per unit area at time $t = 0$ (cm^{-2})
r_t	radius of nuclei at time t (cm)
u^0	constant for the velocity of radius growth depending on the transport of active material ($cm\,s^{-1}$)
v	velocity of radius growth of nickel nuclei ($cm\,s^{-1}$)
v_{OH}	velocity of radius growth of hydroxide ($cm\,s^{-1}$)
v^0	constant for the velocity of radius growth of nickel nuclei depending on the exchange current density ($cm\,s^{-1}$)
v^0_{OH}	constant for the velocity of radius growth of hydroxide depending on the concentration of hydroxyl ions ($cm\,s^{-1}\,dm^6\,mol^{-2}$)
v_1	rate of growth corresponding to the first nucleation regime for nickel [1] ($cm\,s^{-1}$)
v_2	rate of growth corresponding to the second nucleation regime for nickel [1] ($cm\,s^{-1}$)
V_M	molar volume of the deposit ($cm^3\,mol^{-1}$)
V_t	volume of the deposit per unit area at time t (cm)

Greek symbols

α	charge transfer coefficient
β	factor for pH change against current density ($cm^2\,A^{-1}$)
Δt	time step for the numerical calculation (s)
η	overpotential (V)
η^*	nucleation overpotential constant (V)

1. Introduction

Nickel deposition in acidic baths has been widely studied and much work has been devoted to the study of the mechanism of the deposition process [1–3]. Valuable information has been obtained from transient electrochemical techniques. Amblard *et al.* [4] have shown that chronoamperometry is a useful tool

* Unité Mixte de Recherche 7612, Centre National de la Recherche Scientifique.

0021-891X

to investigate nucleation and growth kinetics. The initial stage of nickel formation was explained in terms of three dimensional nucleation [5]. Additional investigation by means of transmission electron microscopy showed that growing centres have a hemispherical shape due to a radial multiple twinning process [6]. Depending on conditions, morphology, compactness and grain size varied.

Electrodeposition of nickel involves a significant amount of hydrogen coevolution, which may, in part, be incorporated within the deposit. This results in the electrodeposited material being very brittle [7]. To avoid this drawback, less acidic solutions can be used. However, Cooper *et al.* [8] have shown that the local pH increases significantly during electrolysis. The local pH change is a major limiting factor for electrolysis at high current density. Nickel oxide or hydroxide is formed at the electrode surface and perturbs the nickel deposition. Indeed, it is known that the stability of $Ni(OH)_2$ is very high [9]. The overall deposition process is rendered more irreversible as a result.

The objective of this paper is to present a model for the potentiostatic transients in order to obtain a quantitative interpretation of the crystallization process occurring at the electrode surface. The role of codeposition of nickel hydroxide is examined. Scanning electron micrography is used to obtain additional information on the morphology of the deposits.

2. Experimental details

Electrochemical experiments were performed in a conventional three-electrode cell. The working electrode was a rotating disc electrode (RDE) with interchangeable bolt holders. Titanium electrodes used in this work were hand made, machined from a rod 3 mm in diameter (Johnson Matthey, 99.99%) and inserted in a Teflon holder. Some experiments were made with glassy carbon (V25, Le Carbone Lorraine). The electrode surface was mechanically polished with successively finer grades of emery paper and alumina powder to 0.05 μm. They were ultrasonically rinsed for 2 minutes in water. The electrodes thus obtained were mirror finished and free from scratches. The rotation speed of the working electrode was 1200 rpm. A jacketed beaker maintained the desired temperature within $\pm 1\,^{\circ}C$ with a total electrolyte volume of 200 ml. The counter and reference electrodes were a large area nickel foil and a saturated calomel electrode (SCE), respectively. The electrochemical measurements were made using an EGG 362 scanning potentiostat coupled with a PAR (model 175) universal programmer. Current transients were recorded by a Nicolet (model 3901) digital oscilloscope. A Tacussel analytical rotator was used. Shielded coaxial cables were used throughout the system to minimize pickup noise. The ohmic resistance was estimated using the current interrupt technique.

Most of the experiments were carried out in an aqueous solution containing 150 g dm^{-3} $NiSO_4.6H_2O$, 45 g dm^{-3} $NiCl_2.6H_2O$ and 50 g dm^{-3} H_3PO_4. To study the influence of pH, a solution containing 26.3 g dm^{-3} $NiSO_4 \cdot 6H_2O$ and 24 g dm^{-3} $NiCl_2 \cdot 6H_2O$ was used, the pH was adjusted by addition of phosphoric acid. The solutions were prepared with analytical-grade reagents and triply distilled water. The morphology of the deposits was examined with a Leica S440 scanning electron microscope using secondary emission.

3. Results

3.1. *Chronoamperometry*

On glassy carbon and titanium electrodes the shape of the j/t transients is similar to that predicted by the classical theory developed by Abyaneh [10]. A typical chronoamperogram for the deposition of nickel on glassy carbon is shown in Fig. 1. The shape of the curve is characteristic of the current response in acidic media, with a S-shaped initial part. At longer time, the current density reaches a smooth maximum and then tends assymptotically toward a limit. Four parts are visible: (i) during a few ten milliseconds a rapid decrease in the current density is obtained, (ii) the current density remains at a low value, (iii) a rapid rising occurs up to a smooth maximum, (iv) then a slow decrease is observed towards an assymptotic limit. The parameters describing the different parts (slope of the rising part, position of the maximum, value of the limit current density) depend on the experimental factors: potential step, temperature, pH.

3.1.1. Potential step. Before the potential pulse the electrode is held at a potential E_s (generally, $E_s = 0.15$ V). Then, the potential is abruptly changed

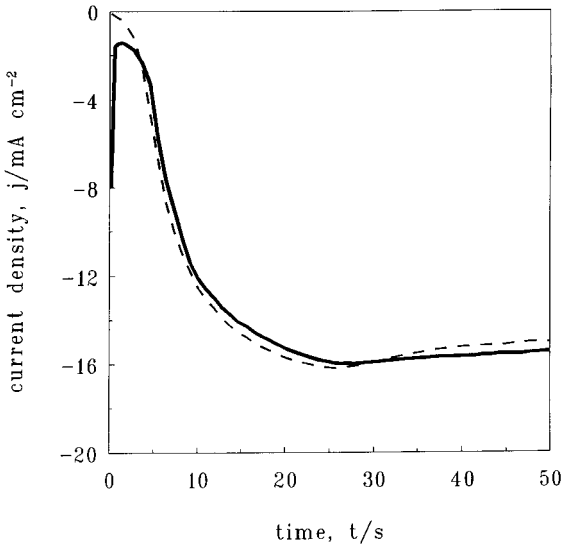

Fig. 1. Chronoamperograms for the nickel deposition on a glassy carbon electrode. Temperature: 40 °C. Potential: −0.95 V vs SCE. (——): experimental; (- - - -): calculated.

to a negative value, E_j. For a potential, $E_j > -0.8\,V$, the current density remains very small and the transients are not reproducible. In the potential range, $-0.8\,V > E_j > -1.2\,V$, a significant increase in the current density is obtained. For $E_j < -1.3\,V$, the influence of the potential on the value of the current density is less sensitive and oscillations due probably to gas evolution appear. Most of the present experiments were carried out in the potential range $-0.8\,V > E_j > -1.2\,V$.

The curves in Fig. 2 illustrate the influence of the potential jump, E_j. When the potential becomes more cathodic, not only does the current density increase but the rise also occurs at a shorter time. This behaviour is obtained for both glassy carbon and titanium. The influence of temperature is similar to that of the potential, a higher temperature induces a more rapid increase in current density.

The chronoamperograms on glassy carbon or titanium have the same shape (Fig. 3). Generally the values of the current density obtained on a glassy carbon electrode are smaller than those on titanium.

3.1.2. Influence of the pH. In acidic solutions (pH $\sim$ 1), the maximum in the current density, if any, always remains very smooth. At higher pH, the shape of the curves changes significantly. As shown in Fig. 4, a well marked maximum appears at pH greater than 4. For the same experimental conditions (temperature, potential jump, electrode material) the initial part of the curve is similar to that obtained in more acidic solutions. However, the rising part stops rapidly and the current density decreases toward a limit much smaller than in acidic solutions. For a potential jump at $-1.15\,V$, the maximum in the potential remains very smooth or disappears for pH lower than 4. A change in the rotation speed in the range 1000–2000 rpm does not modify the results significantly.

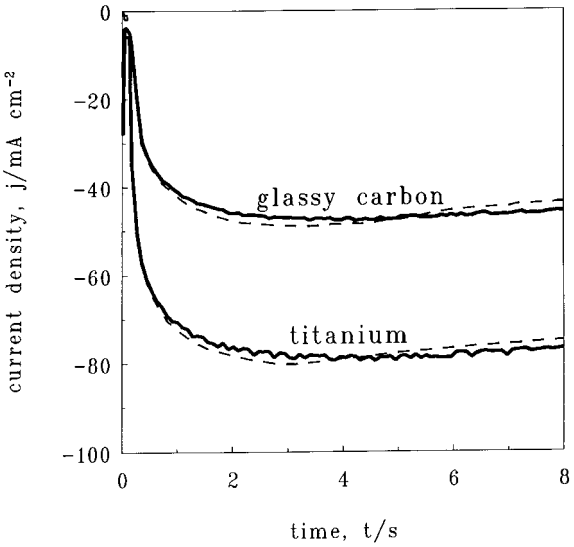

Fig. 3. Chronoamperograms for the nickel deposition on a titanium electrode and a glassy carbon electrode. Temperature: 40 °C. Potential: −1.05 V vs SCE. Continuous line: experimental; dashed line: calculated.

3.2. *Surface morphology*

On titanium or glassy carbon electrodes in acidic solutions, when the electrode is removed from the electrolyte before the end of the rising current, micrographs show the presence of nickel granules at the electrode surface (Fig. 5). Their number depends on the potential step and on the time. For deposits carried out at $E_j = -0.95\,V$, at a time $t = 3\,s$, the mean size of the nickel nuclei is about 0.2 μm, their density lies between 1×10^8 and 5×10^9 nuclei per cm^2 (Fig. 6).

At longer times, after the current maximum, the nuclei coalesce. Crystallized, uniform and fine-grained deposits were observed. At low overpotentials, grey metallic deposits were always found. The higher overpotential the higher nucleus density. The

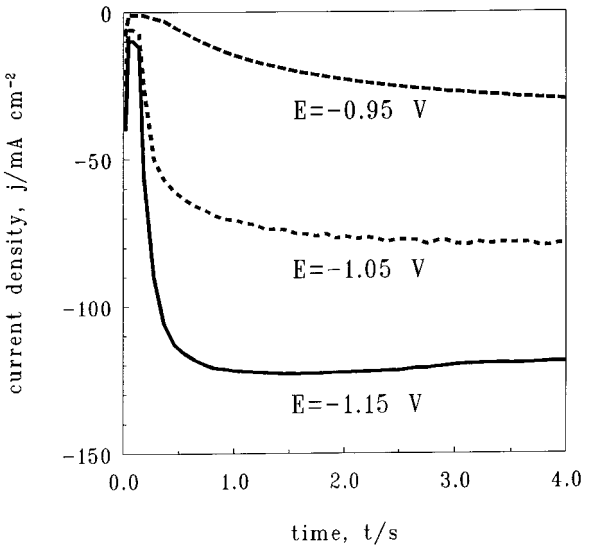

Fig. 2. Chronoamperograms for the nickel deposition on a titanium electrode at various potentials E vs SCE. Temperature: 40 °C.

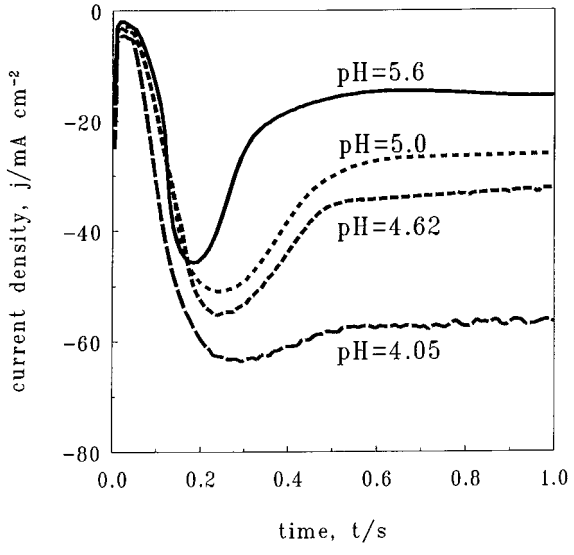

Fig. 4. Chronoamperograms for the nickel deposition on a titanium electrode at various pH. Temperature: 40 °C. Potential: −1.15 V vs SCE.

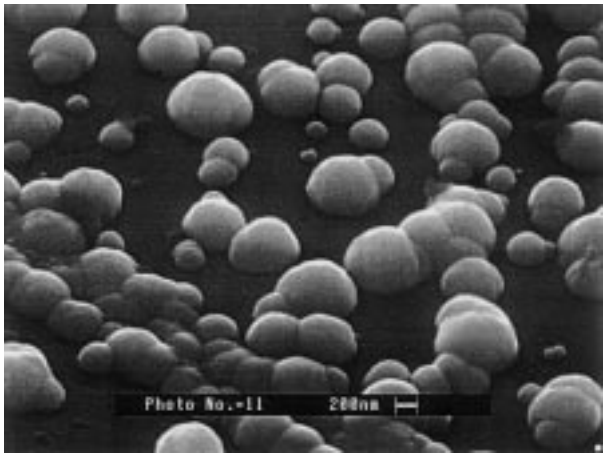

Fig. 5. Scanning electron micrograph of a deposit on a titanium electrode at a potential −0.95 V vs SCE. Temperature: 40 °C. Deposition time: 3 s. Quantity of electricity: $\sim 35 \times 10^{-3}$ C.

size of crystals decreases when the value of the deposition potential is increased. Cracks are prominent on all the surface examined, indicating that the deposits were highly stressed due to hydrogen evolution during electrolysis [9]. For solution containing no acid, the variation of local pH during the deposition causes hydroxide precipitation and modifies the deposit morphology as reported before [9, 11].

4. Discussion

A great deal of research has been devoted to nickel deposition in acidic solutions. In earlier work [2–6, 12] it was demonstrated that the growth of nickel in acidic solution is mainly controlled by charge transfer. The analysis of current–time transients is a powerful tool to investigate nucleation and growth kinetics. Additional information obtained from scanning electron micrograph indicates that, in most cases, the growing centres have a hemispherical shape often due to a radial multiple twinning process.

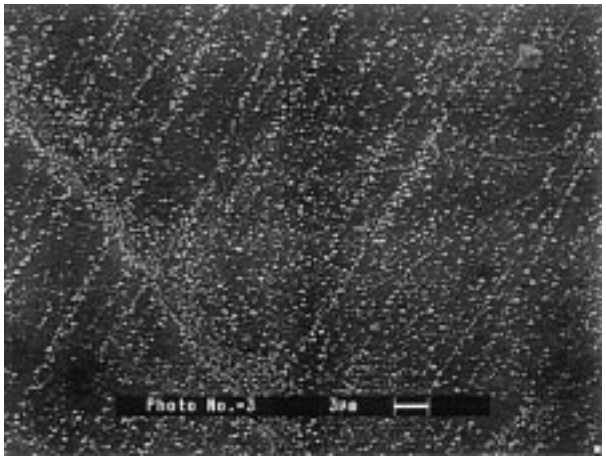

Fig. 6. Scanning electron micrograph of a deposit on a titanium electrode at a potential −0.95 V vs SCE. Temperature: 40 °C. Deposition time: 3 s. Quantity of electricity: $\sim 35 \times 10^{-3}$ C.

4.1. *Modelling*

The chronoamperograms were analysed in the frame of the theory of nucleation and growth centre carried out by Evans [13] and Fleischmann *et al.* [14–16]. This theory has been used by Amblard *et al.* [4] to study nickel deposition in Watts solutions. The model is characterized by the presence of a maximum in the current density and gives a good representation of the experimental curves.

However, some perturbing factors are not included in the theory. Maurin *et al.* [5] have shown that, owing to the ohmic drop between the cathode and the reference electrode, the interfacial potential may vary widely during the potential step. Moreover, the local increase in pH induces a precipitation of nickel hydroxide and perturbs the growth of nickel layer. For these conditions the conventional equations for the current transient are not applicable. Numerical simulation is the only way to treat the problem comprehensively. The outline of the implementation of the finite step difference technique used is described below.

The conversion of a nucleation site into a growing nucleus obeys first order kinetics [5, 16].

$$\Delta N = -kN_{\mathrm{t}}\Delta t \tag{1}$$

As shown from the micrograph in Fig. 5, the nuclei are hemispherical. The radius of the nuclei at time t is given by

$$r_t = r_{t-\Delta t} + v\Delta t \tag{2}$$

At time t there are $n_t (n_t = t/\Delta t)$ families of nuclei. The family j, created at time t_j, is characterized by a radius r_j calculated from Equation 2. At each time step, the area covered with nuclei, if they were allowed to grow independently, is

$$A_t = \pi \sum_{j=1}^{n_t} \Delta N r_j^2 \tag{3}$$

However, the coalescence of adjacent nuclei must be taken into account. According to Evans [13], the fractional area, $\mathscr{A}_t$, covered by nuclei is

$$\mathscr{A}_t = 1 - \exp(-A_t) \tag{4}$$

To calculate the volume of the deposit, the space near the electrode is divided into slices of thickness Δh. The area covered by the deposit in a slice is calculated following the same procedure as for the electrode surface. The area is first calculated without taking coalescence into account. Then, the area actually covered by deposit is calculated according to Equation 4. The volume, V_t, of the deposit is obtained by integrating the contribution of all slices. The current density is given by the charge balance

$$|j_{\mathrm{N_i}}(t)| = nF\frac{V_t - V_{t-\Delta t}}{\Delta t V_{\mathrm{M}}} \tag{5}$$

For constant values of the parameters, k and v, the calculated curves have the shape predicted by theory [15]. It is worth considering the dependence of

parameters on the potential since, during the pulse, the contribution of the ohmic drop varies. According to Wiart [1] the rate of growth obeys a modified Tafel equation which involves two regimes

$$v = \frac{v_1 v_2}{v_1 + v_2} \tag{6}$$

the rates of growth corresponding to the two regimes are

$$\ln v_1 = \ln v_1^0 - b_1\eta \tag{7}$$

and

$$\ln v_2 = \ln v_2^0 - b_2\eta \tag{8}$$

the overpotential is $\eta = E - E^*$. The equilibrium potential obeys the equation, $E^* = E^0 + RT/nF \ln[Ni^{2+}]$ with $E^0 = -0.470$ V vs SCE. Since b_2 is smaller than b_1, and v_2 is greater than v_1 [2], the slope $dv/d\eta$ decreases when the overpotential becomes more negative. The same behaviour is obtained in the present experiments. The results are interpreted in the frame of a charge transfer and surface transport mechanism

$$v = u^0\left\{1 - \frac{u^0 + v^0\exp[(1-\alpha)f\eta]}{u^0 + v^0\exp[-\alpha f\eta]}\right\} \tag{9}$$

v^0 is proportional to the exchange current density and u^0 is the transport coefficient, f is $2F/RT$. At low overpotential and large values of the transport coefficient the reaction is controlled by electron transfer

$$v = v^0\{\exp[-\alpha f\eta)] - \exp[(1-\alpha)f\eta]\} \tag{10}$$

At high overpotential or for a low value of the transport rate, lattice building tends toward the limit, $v \to u^o$. In the present experiments ($\eta < 0$), it is assumed that the term $v^0\exp[(1-\alpha)f\eta]$ is negligible with respect to u^0, and v obeys the equation

$$v = u^0\left\{1 - \frac{1}{1 + \frac{v^0}{u^0}\exp[-\alpha f\eta]}\right\} \tag{11}$$

Many theoretical studies have been devoted to the nucleation process [17]. According to the atomistic model [18] the nucleation rate depends on the frequency with which single adatoms at the electrode surface join nucleation sites. At high overpotentials it is assumed that the equilibrium concentration of adatoms does not depend on the overpotential, and the nucleation rate constant is given by

$$k = K\eta^2\exp -(\eta^*/\eta)^2 \tag{12}$$

4.2. *Hydrogen evolution*

Hydrogen evolution is associated with nickel deposition and depends on the pH [19]. A careful measurement of the faradaic yield has been carried out by Dorsch [20]. The influence of hydrogen evolution was also studied from the comparison of the current transients in electrolyte solutions containing nickel ions with those obtained in solutions which do not contain nickel ions. The experiments show that the fraction of current density due reduction of protons does not depend significantly on the potential, but is strongly affected by the change in pH. This behaviour is in good agreement with previous work [5, 21]. As a first approximation, for pH ≥ 1, the ratio of the current densities due reduction of nickel and protons obeys the equation

$$j_{N_i}/j_{H_2} = \exp(0.4\,\mathrm{pH}) - 1 \tag{13}$$

4.3. *Calculation of the reaction parameters*

The programme ELCRYSIM, based on the finite step process described in Section 4.1, was used to calculate the parameters N^0, v and k. The values of the parameters were adjusted in order to obtain a calculated curve fitting the experimental curve. To take account of the influence of the ohmic drop, the values of the rate constants v and k were varied at each step according to Equations 11 and 12. To avoid oscillations a trial and error procedure was used in order that the current density introduced into the calculation of the ohmic drop, j_tR, was the same as that obtained from the finite step technique at the same time t [22]. The values of the constants v and k for various experimental conditions are reported in Table 1.

Some calculated and experimental curves are shown in Figs 1 and 3. The maximum in the current density expected from the theory of growing nuclei is not always visible. The damping in the maximum is due to the effect of ohmic drop. However, when the pH of the electrolyte is greater than 4, a marked maximum is obtained (Fig. 4). For example, at pH 5.6, the maximum becomes steeper than predicted by theory and cannot be attributed just to the overlapping of growing nuclei. Moreover, the current plateau after the maximum becomes smaller than in more acidic solutions. The decrease in current density is due to formation of nickel hydroxide resulting from local pH change near the interface as pointed out by several authors [8, 9, 23, 24].

Table 1. Values of the reaction parameters in acidic solutions (pH∼1)

Electrode	*Potential* /V	10^{-10} N^{0*} /sites cm^{-2}	k /s^{-1}	10^6 v /cm s^{-1}
Temperature 25 °C				
Ti	−1.15	1.25	88.0	3.35
Ti	−1.05	1.10	40.2	2.90
Ti	−0.95	0.75	12.4	0.36
Temperature 40 °C				
Ti	−1.15	13.5	25.2	5.2
Ti	−1.05	3.4	12.5	5.1
Ti	−0.95	0.5	4.5	2.8
Glassy carbon	−1.15	44.0	12.1	3.7
	−1.05	13.9	6.3	3.1
	−0.95	2.6	2.5	0.5

* N^0 Number of nucleation sites per unit area.

4.4. *Formation of nickel hydroxide*

It is assumed that the formation of nickel hydroxide obeys the same mechanism as described in Section 4.1. The free area for the hydroxide nucleation is given by

$$\mathscr{A}_{OH} = 1 - \exp(-A_{OH}) \quad (14)$$

where A_{OH} is the area covered by nickel hydroxide if no coalescence occurs. The area covered by nickel outside the hydroxide is

$$\mathscr{A}_{Ni} = [1 - \exp(-A_{Ni})]\exp(-A_{OH}) \quad (15)$$

The free area for nucleation of nickel is calculated by taking account of the presence of both nickel and nickel hydroxide

$$\mathscr{A}_{free} = \exp -(A_{OH} + A_{Ni}) \quad (16)$$

Only the nickel nuclei not covered with nickel hydroxide can continue to grow. The nucleation and growing rates of the hydroxide depend on the concentration of hydroxyl ions. The solubility product of nickel hydroxide is $[Ni^{2+}][OH^-]^2 = 5.5 \times 10^{-16}$. The pH_p of incipient precipitation for a 0.1 M Ni^{2+} solution works out to be 6.8, the concentration of OH^- corresponding to the precipitation is $[OH^-]_p = 7 \times 10^{-8}$. For a pH greater than pH_p, the rate of growth is assumed to be proportional to the square of the excess concentration of hydroxide ions, $[OH^-]_{exc} = [OH^-] - [OH^-]_p$.

$$v_{OH} = v^0_{OH}[OH^-]^2_{exc} \quad (17)$$

The nucleation rate constant increases when the pH becomes greater than pH_p. The results show that a linear relationship exists between k_{OH} and $[OH^-]_{exc}$

$$k_{OH} = K_{OH}[OH^-]_{exc} \quad (18)$$

No quantitative indication is given in the literature concerning the relationship between the local pH_s and the current density. We assumed that pH_s is proportional to the current density according to the equation

$$pH_s = pH - \beta j_{N_i} \quad (19)$$

The parameters in Equations 17, 18 and 19 were varied to fit the calculated curves with the chronoamperograms obtained at different pH. Some calculated curves are shown in Fig. 7. The values of the parameters are reported in Table 2. For j in A cm^{-2}, the factor β in Equation 19 is 70.

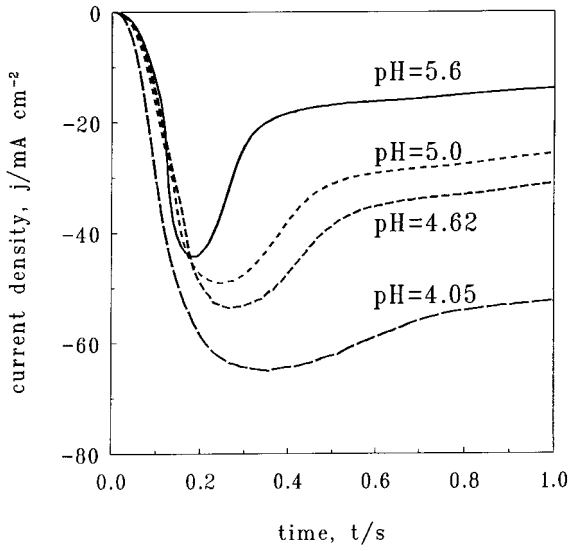

Fig. 7. Calculated chronoamperogram for the nickel deposition on a titanium electrode at various pH. Temperature: 40 °C. Potential: −1.15 V vs SCE.

The results show that an increase in pH induces an increase in both nucleation and growth rates of the hydroxide deposit. Then, a stable phase made of nickel hydroxide appears at the electrode surface as shown by the scanning electron micrograph in Fig. 8. The greater the pH the larger the area covered by hydroxide. Then, passivating zones are formed at the electrode surface. This results in a rapid decrease in the current density and a halt in the growth of the hydroxide layer.

5. Conclusion

A potentiostatic model for the electrodeposition of nickel at a rotating electrode was developed. Special attention was devoted to the effect of the ohmic drop which affects the general shape of the transient and damps the maximum in the current transients. It was shown that nickel deposition in acidic solution on glassy carbon or titanium obeys a nucleation and hemispherical growth process.

When potentiostatic deposition at different pH is compared, the current density is reduced at higher

Table 2. Values of the reaction parameters for the nickel deposition on a titanium electrode at various pH

Temperature: 40 °C; potential, E = −1.15 V vs SCE; pH_m: maximum of the surface pH. k_{OH_m} and v_{OH_m}: calculated values of the nucleation rate and velocity of the hydroxide growth at pH_m.

pH of the solution	$10^{-10}N^{0*}$ /sites cm^{-2}	k /s^{-1}	$10^6 v$ /cm s^{-1}	pH_m (surface)	k_{OH_m} /s^{-1}	$10^4 v_{OH_m}$ /cm s^{-1}
5.6	14.0	21.0	4.7	7.32	24.9	3.2
5.0	9.6	20.8	5.9	7.30	20.0	2.4
4.6	8.6	17.8	5.9	7.29	18.1	2.3
4.1	8.7	18.0	7.7	7.24	17.5	1.9

* N^0 Number of nucleation sites per unit area.

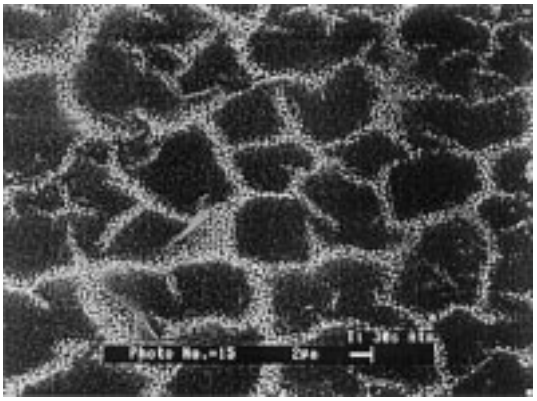

Fig. 8. Scanning electron micrograph of a deposit on a titanium electrode at a potential −1.05 V vs SCE. pH 5.6. Temperature: 40 °C. Deposition time: 10 s. Quantity of electricity: ~0.1 C.

pH, in agreement with previous results [9]. In neutral unbuffered solutions, a poorly conductive layer of nickel hydroxide is formed early because of the oxygen reduction which occurs prior to nickel deposition. The surface $Ni(OH)_2$ inhibits partly the charge transfer reaction and diminishes the nucleation and growth of nickel. The results obtained in the present paper show the influence of pH change at the beginning of the deposition process. The transitory change in pH induces first the formation of a layer of hydroxide [9] which partly covers the electrode surface. Subsequently, there is a decrease in the current, the surface pH becomes again more acidic and the nickel deposition occurs on the uninhibited part of the electrode. The scanning electron micrograph (Fig. 8) shows that nickel flakes are formed, which, according to Gomez *et al*. [11], indicates that deposition occurs with little inhibition. By introducing the concept of partial coverage by nickel hydroxide, the present work provides a link between the two concepts of inhibited and uninhibited nickel deposition in aqueous solutions.

Acknowledgement

This work was partly supported by a cooperation programme between CNRS (France) and CNR (Maroc). The authors would like to thank Dr G. Maurin for fruitful discussions. They are grateful to Dr Beaunier and S. Borensztajn (UPR 15, CNRS) for scanning electron micrography.

References

[1] R. Wiart, Doctorate thesis, Université de Paris, Oberfläche-Surface **9** (1968) 275.
[2] I. Epelboin and R. Wiart, *J. Electrochem. Soc.* **118** (1971) 1577.
[3] I. Epelboin, M. Jousselin and R. Wiart, *J. Electroanal. Chem.* **119** (1981) 61.
[4] J. Amblard, M. Froment, G. Maurin, D. Mercier and E. Trevisan-Pickacz, *ibid.* **134** (1982) 354.
[5] E. Trevisan-Souteyrand, G. Maurin and D. Mercier, *ibid.* **161** (1984) 31.
[6] G. Maurin, 'Growth and Properties of Metal Clusters' (edited by J. Bourdon), Elsevier, Amsterdam, (1980), p.101.
[7] R. L. Zeller III and U. Landau, *J. Electrochem. Soc.* **137** (1990) 1107.
[8] J. H. C. Cooper, D. B. Dreisinger and E. Peters, *J. Appl. Electrochem.* **25** (1995) 642.
[9] C. Q. Cui and J. Y. Lee, *Electrochim. Acta* **40** (1995) 1953.
[10] M. Y. Abyaneh, *ibid.* **27** (1982) 1329.
[11] E. Gómez, C. Muller, W. G. Proud and E. Vallés, *J. Appl. Electrochem.* **22** (1992) 872.
[12] C. Kollia, N. Spyrellis, J. Amblard, M. Froment and G. Maurin, *ibid.* **20** (1990) 1025.
[13] U. R. Evans, *Trans. Faraday Soc.* **41** (1945) 365.
[14] M. Fleischmann and M. R. Thirsk, *Electrochim. Acta* **1** (1959) 146.
[15] M. Y. Abyaneh and M. Fleischmann, *ibid.* **27** (!982) 1513.
[16] *Idem*, *J. Electrochem. Soc.* **138** (1991) 2491.
[17] F. Lantelme, 'Electrocrystallization of Metals from Molten Salts' (edited by D. Shuzhen and Q. Zhiyu), Metallurgical Press, Beijing, China, (1990), pp. 239–65.
[18] Yu. M. Polukarov and A. I. Danilov, *Electrokhimiya* **20** (1984) 374.
[19] C. Arkam, V. Bouet, C. Gabrielli, G. Maurin and H. Perrot, *J. Electrochem. Soc.* **141** (1994) L103.
[20] R. K. Dorsch, *J. Electroanal. Chem.* **21** (1969) 495.
[21] J. L. Carbajal and R. E. White, *J. Electrochem. Soc.* **135** (1988) 2952.
[22] F. Lantelme, A. Seghiouer, Y. Berghoute and J. Chevalet, 'Fundamental Aspects of Electrochemical Deposition and Dissolution Including Modeling' (edited by M. Paunovic, M. Datta, M. Matlosz, T. Osaka and J. B. Talbot), **PV 97–27**, The Electrochemical Society Proceedings Series, Pennington, NJ (1997), in press.
[23] E. Gómez, R. Pollina and E. Vallés, *J. Electroanal. Chem.* **386** (1995) 45.
[24] L. T. Romankiw, 'Electrodeposition Technology, Theory and Practice' (edited by L. T. Romankiw and D. R. Turner), **PV 87–17**, The Electrochemical Society Proceedings Series, Pennington, NJ (1987), p 301.